Resonant electron tunneling through defects in GaAs tunnel diodes

K. Jandieri,[1,a)] S. D. Baranovskii,[1] O. Rubel,[1] W. Stolz,[1] F. Gebhard,[1] W. Guter,[2] M. Hermle,[2] and A. W. Bett[2]
[1]*Department of Physics and Material Sciences Center, Philipps University Marburg, D-35032 Marburg, Germany*
[2]*Fraunhofer Institute for Solar Energy Systems, Heidenhofstr. 2, D-79110 Freiburg, Germany*

(Received 15 May 2008; accepted 23 September 2008; published online 10 November 2008)

Current-voltage characteristics of GaAs tunnel diodes are studied experimentally and theoretically. In theoretical calculations contributions of three different transport mechanisms are considered: direct tunneling processes, nonresonant multiphonon tunneling processes via defects, and resonant tunneling processes through defects. The comparison between theoretical results and experimental data reveals resonant tunneling as the dominant transport mechanism at voltages corresponding to the peak current. At higher voltages this mechanism is replaced by nonresonant tunneling, which is in its turn replaced by over-barrier transport at even larger voltages. © *2008 American Institute of Physics*. [DOI: 10.1063/1.3013886]

I. INTRODUCTION

Tunnel diodes have been the subject of intensive experimental and theoretical studies for the past decades. The investigation of tunnel diode systems is based on their applications in various semiconductor devices, such as digital logic and high-frequency oscillators as well as series connections between tandem solar cells. Monolithically stacked multijunction solar cells based on III–V semiconductor materials[1] can exploit the solar spectrum very profitably and hence have reached high efficiencies of up to $\eta=40.7\%$.[2] The electrical interconnection element for the individual subcells is a critical component of such multijunction solar cells. A high-quality tunnel diode, exhibiting both high optical transparency and low electrical resistivity, would be a good candidate for this task. In our work we studied current-voltage characteristics of GaAs tunnel diodes experimentally and theoretically.

An adequate theoretical description of the current-voltage characteristic requires the correct identification of the dominant tunneling mechanism for different applied voltages. The theoretical basis of tunneling mechanisms and their application to various devices has been studied in numerous papers (see, for example, Refs. 3–13). The three important transport mechanisms are band-to-band, phonon-assisted, and resonant tunneling. In many cases the measured tunneling current is too large to be explained by the direct band-to-band tunneling process. Tunneling through defect states in a space-charge layer of the junction in the device is therefore considered as the dominant transport mechanism. The latter process can be performed as defect-assisted multiphonon tunneling[3–10] or as resonant tunneling through defects.[5,11–13] For instance, for programmable oxide-nitride-oxide read only memories it has been shown that band-to-band tunneling is negligible, while tunneling via defects dominates the charge leakage across the oxide-nitride-oxide sandwich structure.[5] The electrons stored on the floating gate were captured by traps in the 100 Å wide bottom oxide and subsequently emitted into the nitride layer by multiphonon-assisted or resonant tunneling processes. For comparatively low electric fields, multiphonon-assisted tunneling plays the dominant role, while for higher fields resonant tunneling takes over.[5] Tunneling processes via defects were also shown to be important for carrier recombination in $Hg_{0.8}Cd_{0.2}Te$ n^+p junctions with a trap concentration of $N_t=10^{18}$ cm^{-3}.[3] Furthermore in Si the trap-assisted tunneling mechanism was shown to be more important than direct band-to-band tunneling in a wide range of applied voltages.[4] It was also found that resonant tunneling through oxide defects can essentially enhance the gate leakage currents through thin SiO_2 gates in metal-oxide semiconductor field-effect transistors with an oxide thickness smaller than 15 Å at area defect densities larger than 10^{11} cm^{-2}.[6–8] According to Refs. 9 and 10 a significant increase in current in a *p-n* diode is evident at zero-bias depletion layer widths of less than about 300 Å or, equivalently, above a dopant concentration of several 10^{18} cm^{-3}. This increase in current is due to trap-assisted tunneling. In Ref. 11 it was shown that the impurities in the insulating layer of a metal-insulator-metal junction can enhance the conductance of the junction due to resonant tunneling and that intentional high-concentration doping can be used to adjust the conducting properties of the junction in a predictable manner. In Ref. 12 it was suggested that resonant tunneling through defect-related states is an important mechanism for high-field carrier injection into thin SiO_2 films of metal-oxide-semiconductor structures and for high-field insulator breakdown.

In this work we have applied all above-mentioned tunneling mechanisms in order to explain theoretically the current-voltage characteristic of *n*-GaAs/*p*-GaAs tunnel diodes obtained in our experimental studies. It will be shown that resonant tunneling via defect-related states in the depletion layer of the junction is the dominant mechanism responsible for the high peak current in the diode at low applied forward voltages. Section II addresses the experimental data.

[a)]Electronic mail: kakhaber.jandieri@physik.uni-marburg.de. Tel.: +49(0) 6421 2824159. FAX: +49(0) 6421 2827076.

Section III represents the theoretical models used in our calculations. A current-voltage characteristic of the tunnel diode is calculated in Sec. IV. Finally, conclusions are given in Sec. V.

II. EXPERIMENTS

An AIXTRON multiwafer metalorganic vapor phase epitaxy reactor (AIX2600 G3) with $8\times4''$ configuration was used to grow the tunnel diode structures on (100) Ge substrates. The *n*-GaAs and *p*-GaAs layers were highly doped with Te ($N_d=1\times10^{19}$ cm^{-3}) and C ($N_a=3\times10^{19}$ cm^{-3}), respectively. About 1% of In was added to the GaAs in order to achieve lattice match to Ge. Ellipsometric characterization confirmed the optical parameters to correspond well to those of GaAs in the literature.[14] In the following these $Ga_{0.99}In_{0.01}As$ layers will be referred to as GaAs. The tunnel diode devices have been processed by common wet-chemical processing. They were etched to mesa structures with 0.7 mm diameter and plated with metal contacts on top and bottom. The current-voltage (*I-V*) characterization presented in Fig. 8 by solid circles was performed via a four-wire measurement technique at 25 °C without illumination (dark IV). More than 50 different diodes with different areas have been measured and reproduce all well. A peak current density of 21.0 ± 3.8 A/cm^2 was determined.

III. THEORETICAL MODELS

In this section, we describe the theoretical model of the junction used in our calculations and present the tunneling mechanisms. Calculations of the transmission coefficient were performed by the global transfer matrix (GTM) technique described below.

A. Theoretical model of a junction

We consider the tunnel diode as an abrupt junction of degenerate *n*-type and *p*-type semiconductors. Coordinate dependences of the conduction and valence band edges $E_c(x)$ and $E_v(x)$ across the depletion layer of the junction are given by[15]

$$E_c(x)=\begin{cases} E_{c,0}^{(n)}+\dfrac{2\pi e^2}{\epsilon_n}n_0x^2, & x<d_n \\ \Phi-\dfrac{2\pi e^2}{\epsilon_p}p_0(d-x)^2, & d_n\le x<d, \end{cases}$$

$$E_v(x)=\begin{cases} E_c(x)-E_g^{(n)}, & x<d_n \\ E_c(x)-E_g^{(p)}, & d_n\le x<d, \end{cases} \tag{1}$$

where $\Phi=E_g^{(p)}-E_{c,0}^{(n)}+E_{v,0}^{(p)}-U_{\rm app}$, e is the elementary charge, $U_{\rm app}$ is the applied voltage, $E_g^{(n)}$ and $E_g^{(p)}$ are the band gaps, and ϵ_n and ϵ_p are the dielectric permittivities of the *n* and *p* materials, respectively (for a homojunction $E_g^{(n)}=E_g^{(p)}=E_g$ and $\epsilon_n=\epsilon_p=\epsilon$). $d=d_n+d_p$ represents the total thickness of the junction, whereas d_n and d_p are the thicknesses of the depletion layers in the *n*-type and *p*-type semiconductors, respectively, given by

$$d_n=\sqrt{\frac{\epsilon_n\epsilon_p p_0 U}{2\pi e n_0(\epsilon_n n_0+\epsilon_p p_o)}}, \tag{2a}$$

$$d_p=\sqrt{\frac{\epsilon_n\epsilon_p n_0 U}{2\pi e p_0(\epsilon_n n_0+\epsilon_p p_o)}}. \tag{2b}$$

$U=U_c-U_{\rm app}$, where U_c is the contact potential difference. n_0 and p_0 are the concentrations of major charge carriers in the bulk of the *n*-type and *p*-type semiconductors, respectively.

We assume that the distribution of electrons and holes on each side of the junction is given by the Fermi distribution with appropriate quasi-Fermi levels F_n and F_p. For the *n*-type and *p*-type degenerate semiconductors they can be calculated according to[15]

$$F_n=E_{c,0}^{(n)}+k_0T\left(\frac{3\sqrt{\pi}}{4N_c}n_0\right)^{2/3}, \tag{3a}$$

$$F_p=E_{v,0}^{(p)}-E_{c,0}^{(n)}-U_{\rm app}-k_0T\left(\frac{3\sqrt{\pi}}{4N_v}p_0\right)^{2/3}, \tag{3b}$$

where N_c and N_v are the densities of states in the conduction and valence bands, respectively; $E_{v,0}^{(p)}$ is the valence band edge in the bulk of the *p*-type semiconductor. Note that all energies are measured from the conduction band edge $E_{c,0}^{(n)}$ in the bulk of the *n*-type semiconductor and all coordinates are measured from the starting point of the depletion layer in the *n*-type semiconductor.

B. Tunneling mechanisms

Tunneling currents through the *n*-GaAs/*p*-GaAs homojunction are calculated on the basis of the following three tunneling mechanisms: direct band-to-band tunneling, defect-assisted multiphonon tunneling, and resonant tunneling via defects.

1. Direct band-to-band tunneling

The probability to tunnel through the potential barrier is determined by the transmission coefficient $T_D(E)$. This quantity depends on the energy E of the charge carriers. We assume the potential V to be a function of only the x coordinate perpendicular to the junction (so the system is translationally invariant in the yz plane). The current density in the tunnel diode $j_{\rm bb}$ related to the tunneling of electrons from the conduction band of the *n*-type semiconductor into the valence band of the *p*-type semiconductor [see Fig. 1(a)] can be calculated according to[16]

$$j_{\rm bb}=\frac{e}{2\pi\hbar}\int_0^{E_{v,0}^{(p)}}[n_{2D}(F_n-E)-n_{2D}(F_p-E)]T_D(E)dE, \tag{4}$$

where

$$n_{2D}(E)=\frac{m_n k_0 T}{\pi\hbar^2}\ln(1+e^{E/k_0T}) \tag{5}$$

represents the density of electrons in a two-dimensional electron gas in the yz plane, m_n is the effective mass, k_0 is the

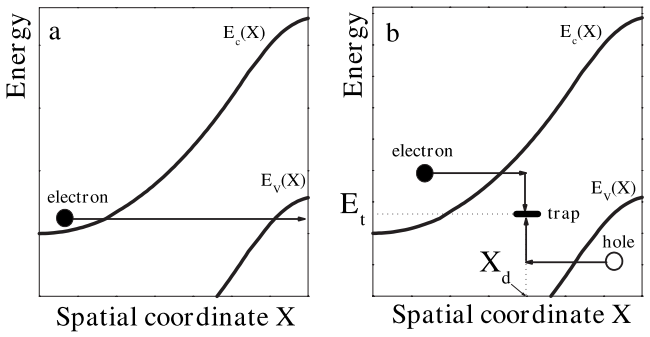

FIG. 1. (a) Schematic representation of direct band-to-band tunneling and (b) nonresonant tunneling through defects.

Boltzmann constant, and T is the lattice temperature.

2. Defect-assisted tunneling

In sufficiently strong electric fields tunneling of electrons (holes) from the conduction (valence) band to the trap state $E_{t,0}$ associated with the defects in the depletion layer of the p-n junction can significantly contribute to the conductance of the junction. According to the recombination model proposed in Refs. 9 and 10 the current density related to the defect-assisted tunneling can be calculated according to

$$j_d = e\int_0^d R_t(x)dx + C, \tag{6}$$

where $C=j_{np}+j_{pn}$ and

$$R_t(x) = \frac{n(x)p(x) - n_i^2}{\frac{\tau_p}{1+\Gamma_p}[n(x) + n_i e^{\bar{E}/k_0T}] + \frac{\tau_n}{1+\Gamma_n}[p(x) + n_i e^{-\bar{E}/k_0T}]}, \tag{7}$$

where p and n denote the local concentrations of free electrons and free holes in the depletion layer of the junction, n_i is the intrinsic carrier concentration, $\bar{E}=E_{t,0}-E_i$ is the difference between the trap level and the middle of the band gap, and τ_n and τ_p are the recombination lifetimes of electrons and holes, respectively. j_{np} and j_{pn} are the electron and hole current densities due to recombination in the neutral p and n regions, respectively. Taking tunneling into account one obtains for the effective recombination lifetimes $\tau_n^{\text{eff}}=\tau_n/(1+\Gamma_n)$ and $\tau_p^{\text{eff}}=\tau_p/(1+\Gamma_p)$, where the factors Γ_n and Γ_p are determined as[9,10]

$$\Gamma_n = \frac{1}{k_0T}\int_0^{\Delta E_n} e^{E/k_0T}T_D(E)dE, \tag{8a}$$

$$\Gamma_p = \frac{1}{k_0T}\int_0^{\Delta E_p} e^{E/k_0T}T_D(E)dE. \tag{8b}$$

These factors account for the effects of phonon-assisted tunneling on the enhancement of both the density of captured carriers by the traps and the emission rates of carriers from the traps. Instead of thermal emission over the entire trap depth, which is the only escape mechanism possible in the absence of an electric field, carriers can also be emitted by the thermal excitation over only a fraction of the trap depth, followed by the tunneling through the remaining potential barrier. So, Γ_n and Γ_p are given by integrals over the trap depth of the product of a Boltzmann factor, which gives the excitation probability of a carrier at the trap level to an excited level E and the tunneling probability at this energy level from the trap to the band. Because of the detailed balance, the same can be said for the recombination process on the trap level [see Fig. 1(b)]. The value of the trap level $E_t(x)=E_c(x)-E_{t,0}$ is position dependent since the conduction band minimum $E_c(x)$ and the valence band maximum $E_v(x)$ are functions of x. Hence, the integration intervals in Eqs. (8a) and (8b) are position dependent. If the trap level $E_t(x)$ lies below the conduction band minimum $E_{c,0}^{(n)}$ at the neutral n side of the junction, tunneling can occur only at an energy level between $E_c(x)$ and $E_{c,0}^{(n)}$ because below $E_{c,0}^{(n)}$ there are no states available that an electron can tunnel from (and into). If the trap level lies above $E_{c,0}^{(n)}$ the integration interval is the whole trap depth, i.e., $\Delta E_n(x)=E_c(x)-E_t(x)$. For holes a similar criterion holds. The expression for the integration intervals can be written as

$$\Delta E_n(x) = \begin{cases} E_c(x) - E_{c,0}^{(n)}, & E_t(x) \le E_{c,0}^{(n)} \\ E_c(x) - E_t(x), & E_t(x) > E_{c,0}^{(n)}, \end{cases}$$

$$\Delta E_p(x) = \begin{cases} E_{v,0}^{(p)} - E_v(x), & E_t(x) > E_{v,0}^{(p)} \\ E_t(x) - E_v(x), & E_t(x) \le E_{v,0}^{(p)}, \end{cases} \tag{9}$$

For week electric fields, when $\Gamma_n,\Gamma_p \ll 1$, formula (7) reduces to the conventional Schokley–Read–Hall recombination mechanism.[17]

3. Resonant tunneling through defects

For resonant tunneling of electrons through defects in a depletion layer of the tunnel diode we use the model proposed in Ref. 13. According to this model, a defect potential energy in a junction can be represented by a square well dividing the whole potential barrier into two regions. Then resonant tunneling through defects can be considered as a double barrier problem. The defect energy level is represented by the resonant tunneling energy level in the system, which can be adjusted by selecting the well width d_W and depth V_W. The electron transmission through a depletion layer with defects is divided into two modes. In the first mode electrons directly tunnel through the area without defects. In the second mode electrons tunnel through the area with a single defect. Combining the two modes of transmission, the total transmission coefficient T_{tot} for one type of defect with the concentration N_t and the constant capture cross section σ is given by[13]

$$T_{\text{tot}}(E,x_d) = \sigma N_t^{2/3}T_{\text{res}}(E,x_d) + (1-\sigma N_t^{2/3})T_D(E), \tag{10}$$

where x_d is the spatial coordinate of the defect and the resonant transmission coefficient $T_{\text{res}}(E,X_d)$ is given by

$$T_{\mathrm{res}}(E,x_d)=\frac{T_1(E,x_d)T_2(E,x_d)}{1+R_1(E,x_d)R_2(E,x_d)-2\sqrt{R_1(E,x_d)R_2(E,x_d)}\cos\Phi}, \tag{11}$$

where $T_1(E,x_d)$, $T_2(E,x_d)$ are the transmission coefficients through the potential barriers surrounding the potential well (representing the defect) at the left and right sides, respectively, $R_1=1-T_1$, $R_2=1-T_2$ are the corresponding reflection coefficients from the barriers, $\Phi=2kd_W+\theta_1+\theta_2$ is the phase angle determined by the electron wave number k in the well, and θ_1, θ_2 are the phase changes during the reflection from the left and the right walls of the well, respectively. The corresponding current density can be calculated again according to Eq. (4) using T_{tot} from Eq. (10) instead of T_D. The resonance takes place at energy E_{res} that satisfies the condition $\Phi=2\pi n$ with integer n. The transmission rises dramatically near the resonance and it reaches its maximum value of unity if the structure is symmetric in the sense that

$$T_1(E_{\mathrm{res}},x_d)=T_2(E_{\mathrm{res}},x_d), \tag{12}$$

when perfect total transmission through the double barrier occurs however opaque the individual barriers are. Condition (12) depends on x_d and thus, this is the case for T_{res}, too. If defects are distributed within a narrow sheet of the depletion layer, such as interfacial defects (surface defects), then the partial contribution of resonant tunneling to the total current is significant only for defects within an extremely narrow range of spatial locations and only a small part of free charge carriers can participate in this process [see Fig. 2(a)]. Any small disturbance of the symmetry condition (12), for instance, by changing the electric field or by shifting the trap position, would damp the resonant transmission peak in a dramatic manner. Therefore, in practical situations these defects should not lead to a significant increase in the tunneling current due to resonant tunneling through defects. Furthermore, our structures have no designed surface doping. Instead, there are uncontrollable defects by impurities in the crystal. To be particular, we assume that there are vacancies related to oxygen that are uniformly distributed in the junction with concentrations of up to $N_t\simeq 10^{15}$ cm^{-3}. Therefore, for an adequate theoretical description of our experimental results, the case of uniformly distributed defects should be considered. In this case a much larger part of free charge carriers can participate in the resonant tunneling process [see Fig. 2(b)] and accordingly, the contribution of resonant tunneling to the total conductance of the diode should be much more significant than in the case of a narrow sheet with defects.

It is worth noting that in the case of the uniform defect distribution, there is also a possibility of tunneling through several defects placed in series. The probability of such "multidefect" tunneling events depends on the ratio $\bar{r}_{\mathrm{def}}/d$, where $\bar{r}_{\mathrm{def}}=N_t^{1/3}$ is a typical distance between defects and d is the thickness of the junction. For typical tunnel diodes, d ranges between 100 and 200 Å. The distance between the defects for $N_t=10^{15}$ cm^{-3} is about $\bar{r}_{\mathrm{def}}=1000$ Å, which is much larger than d. Therefore tunneling through several sequential defects is improbable and we neglect this effect.

C. Global transfer matrix technique

In order to evaluate the transmission coefficient in expressions (4), (8a), (8b), (10), and (11), we use the GTM technique.[18,19] According to this method, the arbitrarily shaped actual potential of width d should be replaced by N rectangular constant potentials V_i of width $d_i=d/N$ (see Fig. 3). The total transmission coefficient of the carrier with energy E_0 can be obtained according to

$$T=\frac{1}{M_{22}}, \tag{13}$$

where M_{22} is determined from the global matrix

$$M=\begin{pmatrix} M_{11} & M_{12} \\ M_{21} & M_{22} \end{pmatrix}. \tag{14}$$

The global matrix, in its turn, is obtained by sequential multiplication of partial transfer matrices, each characterizing the transfer of a free charge carrier through an interface of individual rectangular barriers,

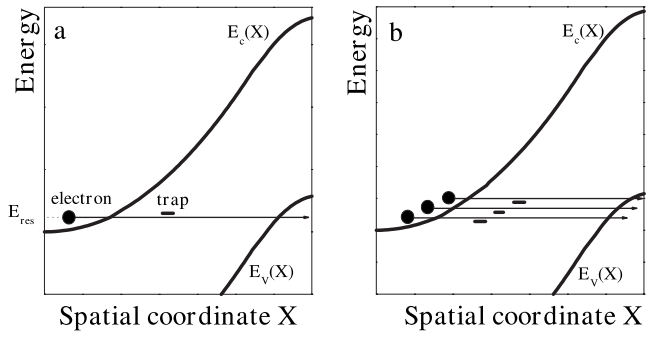

FIG. 2. (a) Schematic representation of resonant tunneling through defects for surface doping and (b) for a homogeneous distribution of defects.

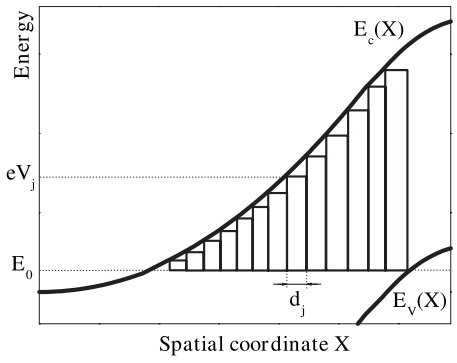

FIG. 3. An arbitrarily shaped actual potential barrier as a set of N rectangular barriers with thickness d_j and height eV_j for the GTM technique.

TABLE I. Parameters of the *n*-GaAs/*p*-GaAs homojunction in thermal equilibrium.

Parameter	Value
N_d	10^{19} cm^{-3}
N_a	3×10^{19} cm^{-3}
E_g [a]	1.43 eV
ϵ [a]	12.9
m_n [a]	$0.063m_e$
m_p^h [a]	$0.051m_e$
m_p^l [a]	$0.082m_e$
d	175 Å
d_n	135 Å
d_p	40 Å
$F_n=F_p$	0.232 eV

[a]Reference 14.

$$M = P_0 \prod_{i=1}^{N} S_i P_i, \tag{15}$$

where

$$S_i = \frac{1}{2}\begin{pmatrix} 1+\frac{k_i}{k_{i-1}} & 1-\frac{k_i}{k_{i-1}} \\ 1-\frac{k_i}{k_{i-1}} & 1+\frac{k_i}{k_{i-1}} \end{pmatrix} \tag{16}$$

characterizes the transfer from region i to $i-1$ and

$$P_i = \begin{pmatrix} \exp(-k_i d_i) & 0 \\ 0 & \exp(k_i d_i) \end{pmatrix} \tag{17}$$

is the matrix for carrier propagation between two interfaces; $k_i=\sqrt{2em(eV_i-E_0)}/\hbar$ is a wave number of the carrier.

IV. CURRENT-VOLTAGE CHARACTERISTICS

In order to calculate the energy diagram of the tunnel diode and to estimate the tunnel currents at given voltages, the values of the material parameters required for the equations given in the previous section have to be determined. For these parameters we take the values gathered in Table I.

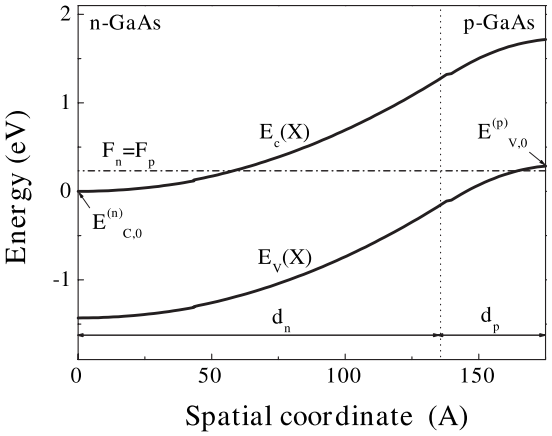

FIG. 4. Energy diagram of the *n*-GaAs/*p*-GaAs homojunction in thermal equilibrium.

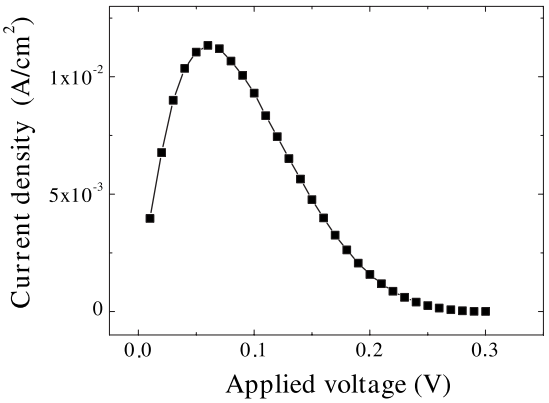

FIG. 5. Current-voltage characteristic of the *n*-GaAs/*p*-GaAs tunnel diode for direct band-to-band tunneling. The line is a guide to the eyes.

The energy diagram of the *n*-GaAs/*p*-GaAs tunnel diode calculated according to Eq. (1) under conditions of thermal equilibrium is presented in Fig. 4.

Calculations performed according to Eq. (4) taking into account only the direct band-to-band tunneling as shown in Fig. 5 result in extremely low tunneling currents as compared to experimental data shown in Fig. 8. Therefore this tunneling mechanism can be neglected in the whole range of the applied voltages.

In order to consider the defect-assisted tunnel current, the energy level of the defect center has to be found. We assume that the major defects in our structures are similar to the oxygen-related defect with energy level $E_{t,0}=0.75$ eV (Ref. 20) homogeneously distributed in the depletion layer of the *n*-GaAs/*p*-GaAs junction.

The values of the current density obtained on the basis of formulas (6) and (7) for the defect-assisted nonelastic tunneling shown in Fig. 6 are much higher than those in the case of the direct band-to-band tunneling (see Fig. 5). In these calculations, the recombination lifetimes of electrons and holes controlled by traps were determined using the relation between the recombination lifetimes and the corresponding recombination coefficients β_n and β_p: $\tau_n=(N_t\beta_n)^{-1}$ and τ_p

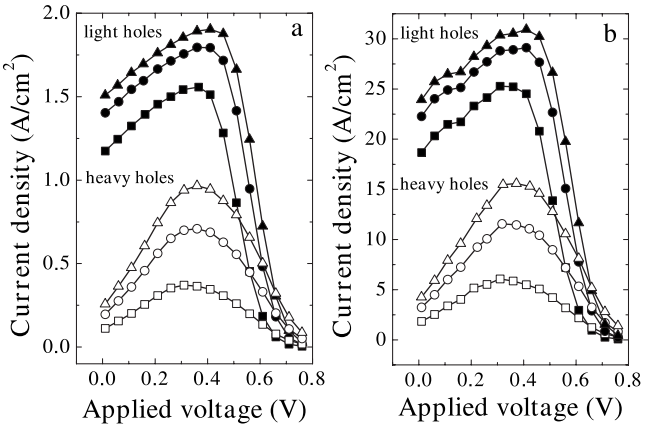

FIG. 6. Current-voltage characteristics of the *n*-GaAs/*p*-GaAs tunnel diode for phonon-assisted tunneling through oxygen-related defects with the defect concentrations (a) $N_t=5\times10^{14}$ cm^{-3} and (b) $N_t=8\times10^{15}$ cm^{-3}, and for different values of β_p: 5×10^{-10} cm^3 s^{-1} (rectangles), 2×10^{-9} cm^3 s^{-1} (circles), and 4×10^{-9} cm^3 s^{-1} (triangles). Lines are guides to the eyes.

$=(N_t\beta_p)^{-1}$. The value $\beta_n \simeq 7\times10^{-9}$ cm^3 s^{-1} is known.[20] The value β_p for oxygen-related centers in GaAs is, however, not known exactly. Figure 6 shows the calculated current-voltage characteristics in cases of light and heavy holes for various values of β_p and N_t. One can see that the variation of β_p in the range $\beta_p \simeq 5\times10^{-10},\ldots,5\times10^{-9}$ cm^3 s^{-1} does not change the current-voltage characteristics essentially and that the current in the case of light holes is significantly higher than for heavy holes. Because of their comparatively large effective radius, the light holes contribute more to the tunnel-assisted currents than heavy holes do. Since the effective mass of light holes $m_p \simeq 0.082m_e$ is only slightly larger than the effective mass of electrons $m_n \simeq 0.063m_e$, and also the oxygen-related energy level in GaAs lies nearly in the middle of the energy gap, the above-considered values of β_p chosen close to β_n seem reasonable. The results are sensitive to the choice of the defect concentration N_t. From comparing the data in Fig. 6 with the experimental results in Fig. 8 one can conclude that the nonresonant tunneling cannot account for the experimental data in the range of voltages corresponding to the maximum of the current. The values of the observed maximum of the current could be achieved assuming the concentration of defects as high as $N_t \simeq 8\times10^{15}$ cm^{-3}. This concentration is unreasonably high. Moreover, even in such a case the voltage corresponding to the maximum of the current would be much higher than the one observed experimentally, as shown in Fig. 8. Furthermore, at such high defect concentrations the resonant tunneling process considered below would give much larger currents than those shown in Fig. 6 and those measured experimentally. Therefore one can exclude the nonresonant current as dominating process in the range of voltages corresponding to the maximum of the current.

Let us now discuss resonant tunneling through defects. According to Eqs. (10) and (11), important parameters for calculation of the resonant tunneling current are the capture cross section σ and the concentration of the defects N_t. The cross section can be determined according to $\sigma=\beta_n(\bar{v}_T)^{-1}$, where $\bar{v}_T$ is the thermal velocity of an isolated electron. For $T=300$ K we have $\sigma \simeq 7\times10^{-16}$ cm^2, which is in good agreement with experimental data.[20]

Using Eqs. (4), (10), and (11), we obtain an *I-V* characteristic shown in Fig. 7 for different concentrations of defects N_t in the range between 10^{14} and 10^{15} cm^{-3}. By comparing these results with the experimental data in Fig. 8 we come to the conclusion that resonant tunneling through defects is able to account for the maximum current at the appropriate applied voltage, provided the concentration of defects in our system is about 5×10^{14} cm^{-3}. Therefore we conclude that resonant tunneling is the dominant transport mechanism at voltages corresponding to the current maximum. Furthermore, a comparison between experimental data and the theoretical calculations allows to estimate the concentration of defects N_t in the sample under study.

For higher voltages the resonant tunneling current decreases rapidly due to the decreasing number of states available for electrons to transfer into the valence band of the *p*-type semiconductor. Under these circumstances phonon-assisted tunneling provides the only possibility for electron

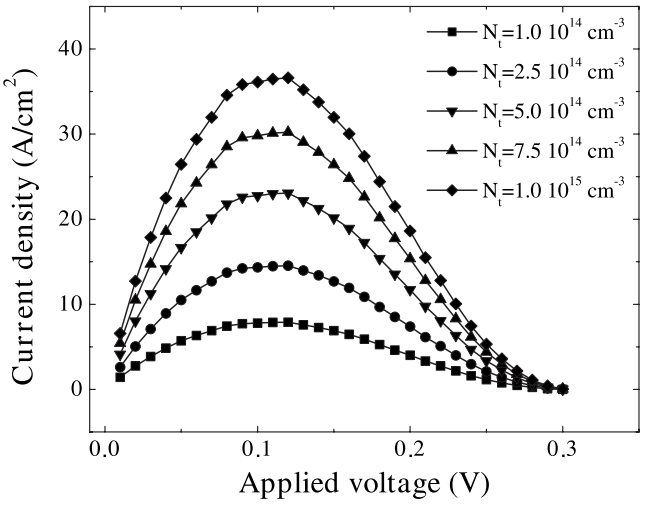

FIG. 7. Current-voltage characteristics of the *n*-GaAs/*p*-GaAs tunnel diode for resonant tunneling through oxygen-related defects with capture cross section $\sigma=7\times10^{-16}$ cm^2 and different defect concentrations: $N_t=1\times10^{14}$ (rectangles), 2.5×10^{14} (circles), 5×10^{14} (down triangles), 7.5×10^{14} (up triangles) and 1×10^{15} (diamonds). Lines are guides to the eye.

tunneling and this process should be taken into account. By further increasing the applied voltage, phonon-assisted tunneling, in its turn, is replaced by overbarrier transport with exponential current-voltage dependence as the dominant mechanism.[15] In the range of intermediate applied voltages, which is larger than the voltage corresponding to the current peak, both phonon-assisted tunneling and overbarrier transport give comparable contributions to the transport process. Therefore, for an adequate description of the experimental data in the range of such intermediate voltages, the overbarrier transport should also be taken into account. This was done in a semiempirical manner. If one uses the logarithmic scale for the experimental *I-V* characteristics shown in Fig. 8, it becomes clear that for $U_{app}>0.8$ V the *I-V* dependence is purely exponential. The extrapolation of this dependence for lower voltages leads to the following expression for the current j_{ob}, related to the overbarrier transport mechanism:

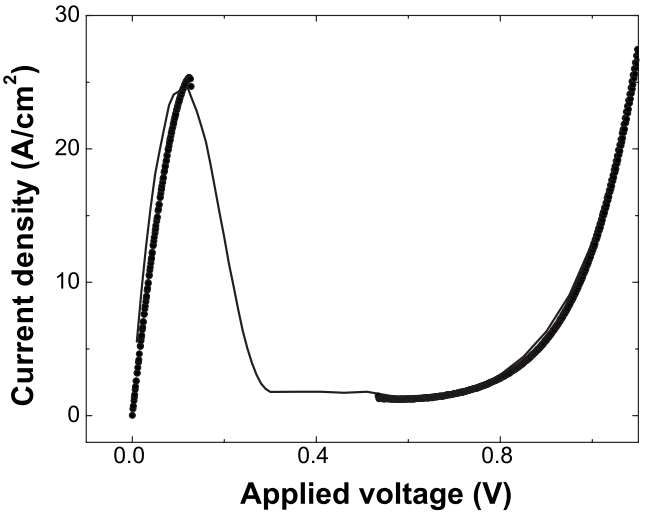

FIG. 8. Theoretical current-voltage characteristic of the *n*-GaAs/*p*-GaAs tunnel diode including all possible transport mechanisms (solid line); $\sigma=7\times10^{-16}$ cm^2, $N_t=5\times10^{14}$ cm^{-3}. Circles represent the experimental data.

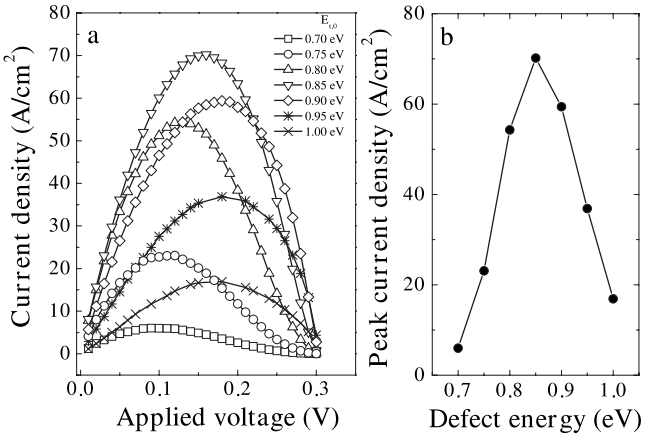

FIG. 9. (a) *I-V* dependences of the *n*-GaAs/*p*-GaAs tunnel diode for resonant tunneling through defects with constant values for the defect concentration $N_t=5\times10^{14}$ cm^{-3} and the capture cross section $\sigma_n=7\times10^{-16}$ cm^2 but with different energy levels: $E_{t,0}=0.70$ eV (rectangles), 0.75 eV (circles), 0.80 eV (up triangles), 0.85 eV (down triangles), 0.90 eV (diamonds), 0.95 eV (stars), and 1.00 eV (crosses); (b) Dependence of peak current on the energy level of the defect. Lines are guides to the eyes.

$$j_{\mathrm{ob}} = A\,\exp(BV_{\mathrm{app}}), \tag{18}$$

with $A\simeq9.68\times10^{-3}$ A cm^{-2} and $B\simeq7.2$ V^{-1}.

Figure 8 represents the current-voltage characteristic calculated by a combination of resonant and nonresonant tunneling through oxygen-related defects (with $E_{t,0}=0.75$ eV), homogeneously distributed in the depletion layer of *n*-GaAs/*p*-GaAs tunnel junction as well as the overbarrier transport mechanism. The best agreement between the theoretical results and experimental data has been obtained for $\beta_p\simeq2\times10^{-9}$ cm^3 s^{-1} and $N_t\simeq5\times10^{14}$ cm^{-3}.

The question that might arise is whether this type of defect, which we considered as the dominant in our sample, provides the highest possible peak currents through the *p-n* GaAs junction. In Fig. 9 we show the result of calculations of the current resulting from defect-assisted resonant tunneling for different positions of the defect energy level, keeping the concentration of defects and the capture cross section equal to those found for the oxygen-related defects. The peak current appears to be a nonmonotonic function of $E_{t,0}$ with a maximum for $\simeq0.85$ eV.

V. CONCLUSIONS

The current-voltage characteristics of *n*-GaAs/*p*-GaAs tunnel diodes as an interconnection element in multijunction solar cells are studied experimentally and theoretically. A high peak current ($\simeq25$ A cm^{-2}) at relatively low applied voltages ($\simeq0.1$ V) is observed. Experimental data were analyzed taking into account direct band-to-band tunneling, phonon-assisted tunneling through defects homogeneously distributed within the depletion layer of the junction, and resonant tunneling through these defects modeled as potential wells surrounded by two potential barriers. For low applied voltages resonant tunneling through defects is shown to be the dominant transport mechanism responsible for the high peak current in the tunnel diode. A good agreement with experimental data has been obtained in the case of oxygen-related defects with an energy level $E_{t,0}=0.75$ eV and concentration $N_t=5\times10^{14}$ cm^{-3}. Direct band-to-band tunneling can be neglected in the whole range of the applied forward voltages. For intermediate values for the applied voltages, phonon-assisted tunneling through defects becomes the dominant transport mechanism. Good agreement with experimental data has been obtained assuming that the light holes play the decisive role in the tunnel-assisted recombination processes and the corresponding recombination coefficient has the same order of magnitude as the recombination coefficient of electrons. For high applied voltages the overbarrier transport mechanism becomes dominant with the conventional exponential current-voltage dependence.

ACKNOWLEDGMENTS

Financial support of the Fonds der Chemischen Industrie, of the Deutsche Forschungsgemeinschaft and of the European Graduate Program "Electron-electron interactions in solids" (Grant No. DFGOTKA GRK790) is gratefully acknowledged. This work was supported in part by the European Commission through the funding of the project FULLSPECTRUM (Grant No. SES6-CT-2003-502620). The work of W.G. is supported by the Deutsche Bundesstiftung Umwelt.

[1] A. Luque and V. M. Andreev, *Concentrator Photovoltaics* (Springer-Verlag, Heidelberg, 2007).
[2] R. R. King, D. C. Law, K. M. Edmondson, C. M. Fetzer, G. S. Kinsey, H. Yoon, R. A. Sherif, and N. H. Karam, Appl. Phys. Lett. **90**, 183516 (2007).
[3] A. Schenk, J. Appl. Phys. **71**, 3339 (1992).
[4] A. Schenk, Solid-State Electron. **36**, 19 (1993).
[5] M. Hermann and A. Schenk, J. Appl. Phys. **77**, 4522 (1995).
[6] M. Stadele, B. Fischer, B. R. Tuttle, and K. Hess, Superlattices Microstruct. **28**, 517 (2000).
[7] M. Stadele, B. R. Tuttle, and K. Hess, J. Appl. Phys. **89**, 348 (2001).
[8] M. Stadele, B. Fischer, B. R. Tuttle, and K. Hess, Solid-State Electron. **46**, 1027 (2002).
[9] G. A. M. Hurkx, D. B. M. Klaassen, and M. P. G. Knuvers, IEEE Trans. Electron Devices **39**, 331 (1992).
[10] G. A. M. Hurkx, H. C. de Graaff, W. J. Kloosterman, and M. P. G. Knuvers, IEEE Trans. Electron Devices **39**, 2090 (1992).
[11] J. W. Gadzuk, J. Appl. Phys. **41**, 286 (1970).
[12] B. Ricco, M. Y. Azbel, and M. H. Brodsky, Phys. Rev. Lett. **51**, 1795 (1983).
[13] C. W. Jiang, M. A. Green, E. C. Cho, and G. Conibeer, J. Appl. Phys. **96**, 5006 (2004).
[14] M. E. Levinshtein and S. L. Rumyantsev, *Handbook Series on Semiconductor Parameters* (World Scientific, London, 1996), Vol. 1.
[15] N. W. Ashcroft and N. D. Mermin, *Solid State Physics* (Holt, Rinehart and Winston, New York, 1976).
[16] L. Esaki, Phys. Rev. **109**, 603 (1958).
[17] C. M. Wolfe, N. Holonyak, and G. E. Stillman, *Physical Properties of Semiconductors* (Prentice-Hall, Engelwood Cliffs, 1989).
[18] R. Redhammer and F. Urban, Phys. Status Solidi B **182**, 133 (1994).
[19] J. Racko, A. Gramova, J. Parizek, and J. Breza, Czech. J. Phys. **47**, 649 (1997).
[20] D. V. Lang and C. H. Henry, Phys. Rev. Lett. **35**, 1525 (1975).